Calhoun
Institutional Archive of the Naval Postgraduate School

Calhoun: The NPS Institutional Archive

DSpace Repository

Theses and Dissertations | 1. Thesis and Dissertation Collection, all items

1968-06

Measurement of the proton form factor at low momentum transfer.

Gordon, Robert H.

Monterey, California. Naval Postgraduate School

http://hdl.handle.net/10945/12630

Downloaded from NPS Archive: Calhoun

http://www.nps.edu/library

Calhoun is the Naval Postgraduate School's public access digital repository for research materials and institutional publications created by the NPS community. Calhoun is named for Professor of Mathematics Guy K. Calhoun, NPS's first appointed -- and published -- scholarly author.

Dudley Knox Library / Naval Postgraduate School
411 Dyer Road / 1 University Circle
Monterey, California USA 93943

NPS ARCHIVE
1968
GORDON, R.

MEASUREMENT OF THE PROTON FORM FACTOR AT LOW MOMENTUM TRANSFER

ROBERT H. GORDON

DUDLEY KNOX LIBRARY
NAVAL POSTGRADUATE SCHOOL
MONTEREY CA 93943-5101

DUDLEY KNOX LIBRARY
NAVAL POSTGRADUATE SCHOOL
MONTEREY CA 93943-5101

MEASUREMENT OF THE PROTON FORM FACTOR AT LOW MOMENTUM TRANSFER

by

Robert H. Gordon
Lieutenant, United States Navy
B. S., Saint Joseph's College, 1959

[redacted]

Submitted in partial fulfillment of the
requirements for the degree of

MASTER OF SCIENCE IN PHYSICS

from the

NAVAL POSTGRADUATE SCHOOL
June 1968

NPS Archive
1968
Gordon, R.

RRD G5748 c.1

ABSTRACT

Electron scattering experiments on the proton were carried out in a range of momentum transfers squared of 0.025 (Fermi^{-2}) to be 0.65 (Fermi^{-2}).

Polyethylene was used as target material and the proton data were normalized against carbon electron scattering data taken at higher momentum transfer.

The relative proton data obtained in this manner do not fit the generally accepted form factor curves.

Possible reasons for the deviations in view of recent suggestions about the existence of a proton halo are offered. However, it is not possible at the present stage of accuracy to make any definite statement except that the data are not inconsistent with the existence of a proton halo.

TABLE OF CONTENTS

Chapter		Page
1	Introduction	9
2	Theory of Electron Proton Scattering	11
3	Proton Form Factor	19
4	Radiative Corrections	21
5	Experimental Setup	23
6	Calculations of Experimental Cross Sections	26
7	Evaluation of Data	31
8	Discussion of Data	33
9	Conclusions	34

LIST OF TABLES

Table		Page
I	The Form Factor as a function of momentum transfer squared (q^2)	32

LIST OF ILLUSTRATIONS

Figure		Page
I	Spectrometer, counter and target arrangement	35
II	Target assembly	36
III	Elastic Scattering peaks of good quality	37
IV	Elastic Scattering peaks of poor quality	38
V	Proton peak unfolded from poor quality elastic peak	39
VI	JANSSENS' Proton Form Factor curve and individual data points	40
VII	JANSSENS' curve, BARRET'S halo curve and averaged data points	41

ACKNOWLEDGEMENTS

The author wishes to express his appreciation to Professor Franz A. Bumiller, the Director of the LINAC group, for his constructive guidance and assistance, and to Professor Fred R. Buskirk for his aid and encouragement. To Mr. F. Ryan for help with computer programming. To Mr. M. O'Dea for assistance in the construction of various experimental equipment.

The author is especially thankful for the willing efforts of Lt. Jake W. Stewart, Lt. Jesse W. Armstrong, Lt. Nicholas M. Ferriter, Maj. Royce D. Miller, USA, and 2ndLt. Lewis P. Gaby II, USAF, members of the LINAC group.

1. INTRODUCTION

As early as 1955 electron-scattering experiments on the proton indicated its structure to be more complicated than that of a point-charge and a point-magnetic moment. For the proton, represented as a point-charge and a point-magnetic moment, the differential scattering cross section is given by Rosenbluth [1].

Deviations from point scattering are usually expressed by a form factor $F(q^2)$ given by the definition [2]

$$F^2(q^2) = \frac{\text{EXPERIMENTAL CROSS SECTION}}{\text{THEORETICAL CROSS SECTION}} .$$

In the case of the proton it becomes necessary to describe the scattering behavior with two form factors $F_1(q^2)$, associated with the Dirac charge, and magnetic moment of the proton, while $F_2(q^2)$ describes the anomalous (Pauli) moment. However, at low values of momentum transfer q, the charge form factor F_1 is highly predominant and contributions from F_2 cannot be detected even with high experimental accuracy.

This work was originally started to obtain values of F_1 at the lowest possible momentum transfers. Such measurements, if sufficiently accurate, allow a model independent determination of the radius of the proton's charge distribution.

While this work was in progress, a publication by Barrett et al [3] gave rise to the speculation that the proton's charge distribution is considerably more complicated than heretofore assumed. Indeed, it was suggested that part of the proton's charge is distributed in the form of a "halo" at distances rather large compared to the proton's mean radius.

Confirmation or denial of such a feature requires an experimental accuracy not yet available in absolute electron scattering experiments. The data obtained in the present study are, however, suggestive enough to warrant a continuation of the effort.

2. THEORY OF ELECTRON PROTON SCATTERING

For electrons scattering from a Dirac proton, the evaluation of the S - matrix elements in covariant perturbation theory of Quantum Electrodynamics can be worked out most rigorously to first order in α (the fine structure constant). This will yield the transition rate and the scattering cross section.

The spinor functions for the electron's field can be defined from the following:

$$\psi(x) = \sqrt{\frac{m}{EV}}\, u(p) e^{-ip_\mu x^\mu} \tag{1}$$

p is the momentum four vector with components p_μ. The current density is given by

$$j^\mu(x) = e\bar{\psi}\gamma^\mu\psi \tag{2}$$

Similiarly the spinor functions for the proton's field can be defined from

$$\Psi(x) = \sqrt{\frac{M}{\epsilon V}}\; w(p) e^{-iP_\nu x^\nu} \tag{3}$$

and by use of the Correspondence principle we can choose the current density of the proton to be

$$J^\nu(x) = e_p\bar{\Psi}\gamma^\nu\Psi \tag{4}$$

where $e_p = -e > 0$. Now, using the Green's Function method to solve the inhomogeneous boundary value problem

$$\partial_\lambda\partial^\lambda A^\nu(x) = J^\nu(x)$$

The electromagnetic field produced by the proton is determined to be

$$A^{\nu}(x) = \int d^4x^1 \, D_F(x-x^1) J^{\nu}(x^1) \tag{5}$$

and the fourier representation of $D_F(x-x^1)$ in momentum space is

$$D_F(x-x^1) = \frac{1}{(2\pi)^4} \int d^4q \, e^{-iq.(x-x^1)} D_F(q^2) \tag{6}$$

where $$D_F(q^2) = \lim_{\mu \to 0} \frac{-1}{q^2 + i\mu}$$

$D_F(x-x^1)$ is proportional to the Feynman electromagnetic radiation propagator in Quantum Electrodynamics, i.e., it is a Green's Function. With substitution of equation (3) into equation (4) and the subsequent substitution of the result into equation (5) along with equation (6), the electromagnetic field of the proton takes the following form

$$A^{\mu}(x_1) = \frac{1}{(2\pi)^4} \int d^4x_1 d^4q \left[\frac{e^{-iq.(x_1-x_2)}}{q^2 + i\mu} \right]$$

$$\times \left[\sqrt{\frac{M^2}{\epsilon_f \epsilon_i}} \frac{e}{V} e^{i(P_f - P_i).x_2} \, \bar{w}(P_f) \gamma^{\mu} w(P_i) \right] \tag{7}$$

Returning to the S-matrix in Quantum Electrodynamics the general form is

$$S = \sum_{n=0}^{\infty} \frac{(-i)^n}{n!} \int_{\text{all space}} d^4x_1 \int d^4x_2 \cdots\cdots \int d^4x_n T \left[H_I(x_1) \cdots H_I(x_n) \right]$$

Where τ is the chronological operator and $H_I(x_j)$ represents the interaction Hamiltonian at the space time point x_j. Now in the particular case of the electron-proton scattering the interaction Hamiltonian is

$$H_I(x) = e\overline{\psi(x)}\gamma^{\mu}\psi(x)A_{\mu}(x)$$

The chronological operator τ is of no consequence when the first order term of the S-matrix is considered and then S^1_{fi} is

$$S^1_{fi} = (-ie) \int d^4x_1 \left[\overline{\psi(x_1)}\gamma^{\mu} \psi(x_1)A_{\mu}(x_1) \right]$$

Substitution of equation (7) into S^1_{fi} yields after some manipulation

$$S^1_{fi} = \frac{1}{(2\pi)^4} \lim_{\mu \to 0} \left\{ - \frac{e^2}{V^2} \sqrt{\frac{m^2M^2}{E_f E_i \epsilon_f \epsilon_i}} \int d^4x_1 d^4x_2 d^4q \; x \right.$$

$$e^{i(p_f - p_i - q).x_1} \left[\bar{u}(p_f)\gamma^{\mu}u(p_i) \right] \frac{1}{q^2 + i\mu} \; x$$

$$\left. \left[\bar{w}(P_f)\gamma_{\mu}w(P_i) \right] e^{-i(P_i - P_f - q).x_2} \right\}$$

and completion of the spatial integrations yields for S^1_{fi}

$$S^1_{fi} = (2\pi)^4 \frac{(-i)}{V^2} \sqrt{\frac{m^2M^2}{E_f E_i \epsilon_f \epsilon_i}} \delta^4(P_f - P_i + p_f - p_i) M^1_{fi} \qquad (8)$$

where

$$M^1_{fi} = \bar{u}\gamma^{\mu}u \; \frac{e^2}{q^2 + i\mu} \; \bar{w}\gamma_{\mu}w$$

$$q^2 = (p_f - p_i)^2 = (P_f - P_i)^2$$

and

$$0 < \mu << 1.$$

The transition probability per unit space-time volume is obtained from

$$\Gamma' = \frac{|S^1_{fi}|^2}{VT}$$

or upon substitution of equation (8) and a little algebra yields

$$\Gamma' = (2\pi)^4 \delta^4 (P_f - P_i + p_f - p_i) \frac{m^2 M^2}{V^4 E_f E_i \epsilon_f \epsilon_i} |M^1_{fi}|^2$$

From Quantum Electrodynamics the cross section for a two particle final state is by definition

$$\frac{d\sigma}{d\Omega} = \frac{\text{Transition probability per unit time}}{\text{Flux of incident particles}}.$$

Γ, which is the probability per unit time for a transition from an initial one particle state to a final state of n particles having any energies, momenta, and spin consistant with conservation laws, can be calculated from Γ' by multiplying by the volume of space, and the phase space factors, summing over the final spins and integrating over the final momenta. The result except for summation and integration is

$$\frac{d\sigma}{d\Omega} = \frac{mM}{\sqrt{(p_i \cdot P_i)^2 - m^2 M^2}} \left|M_{fi}^1\right|^2 (2\pi)^4 \delta^4 (P_f - P_i + p_f - p_i) \times$$

$$\frac{m d^3 p_f}{(2\pi)^3 E_f} \cdot \frac{M d^3 P_f}{(2\pi)^3 \epsilon_f} \tag{10}$$

But for an unpolarized beam of electrons, an average over the initial states must be taken, then the absolute value of the matrix element M_{fi}^1 squared becomes

$$\left|M_{fi}^1\right|^2 = \lim_{\mu \to 0} \frac{1}{4} \sum_{\text{spins}} \left| \bar{u} \gamma^\mu u \frac{e^2}{q^2 + i\mu} \bar{w} \gamma_\mu w \right|^2 \tag{11}$$

Substitution into equation (11) the spinor amplitudes for u(p) and w(p), performing the trace calculations, taking the limit and a considerable amount of laborious algebra finally yields,

$$\left|M_{fi}^1\right|^2 = \frac{e^4}{2m^2 M^2 q^4} \left\{ (P_f \cdot p_f)(P_i \cdot p_i) + (P_f \cdot p_i)(P_i \cdot p_f) \right.$$

$$\left. - m^2 (P_f \cdot P_i) - M^2 (p_f \cdot p_i) + 2M^2 m^2 \right\}$$

Using this result in equation (10), then performing some tedious phase space integration and converting to the laboratory frame where the proton was initially at rest, yields the well known result

$$\frac{d\sigma}{d\Omega} = \frac{e^4 \cos^2 \theta/2}{4E_i^2 \sin^4 \theta/2} \times \frac{1 - \frac{\hbar^2 q^2}{2M^2} \tan^2 \theta/2}{1 + \frac{2E_i}{Mc^2} \sin^2 \theta/2} \tag{12}$$

In obtaining this expression the approximation m^2 (Electron rest mass) $\rightarrow$ 0 has been used ($m_e \ll E_i$). If M (target rest mass) approaches a large value the Mott [4] cross section is produced.

The above cross section is correct if it is assumed that a single virtual photon is exchanged and the proton is a point particle with no anomalous magnetic moment. But it is known that due to the proton meson interactions, hydrogen shows hyper-fine structure. The conclusion is that the proton's magnetic moment is different from that for a Dirac particle (i.e., it is not e/2M). Therefore equation (11) must be modified to take into account

a) the non locality of the interaction because of the nucleon structure

b) the anomalous part of the magnetic moment.

The first modification may be introduced by rewriting $j^{\mu}(x)A_{\mu}(x)$ as $j^{\mu}(x)\ F(x-x^1)A_{\mu}(x)$ where $F(x-x^1)$ is a shape or form factor describing the distribution of charge over the proton. It is usually more convenient to work with invariant momentum transfers rather than spatial functions; so a Fourier transform of $F(x-x^1)$ is introduced

$$F(q^2) = \int d^4x' \ F(x-x') \ e^{-iq.(x-x')}$$

Thus $F(q^2)$ represents a form factor in momentum space, and the proton vertex is therefore changed from a point to a blob (see below)

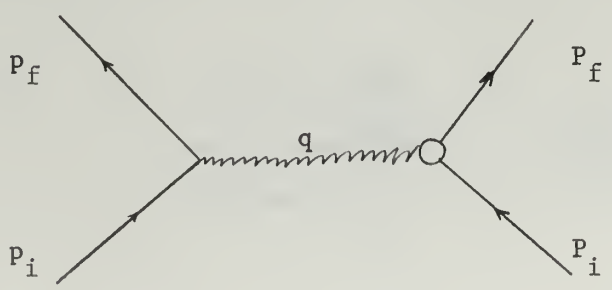

The second modification is obtained by considering the most general form of the matrix element permitted by the requirements of Lorentz transformations and gauge invariance. That is the term $\overline{w}\,\gamma_\mu w$ in equation (11) will be replaced by the most general form for the proton current, namely

$$\overline{w}\,O_\mu w$$

where O_μ is any expression (or group of expressions) which has the transformation properties of a four vector and is also a four by four matrix in the spin space of the proton i.e., it is a function of the four vectors P_f and P_i and the γ matrices. Rather than use P_f and P_i separately, it is convenient to use the linear combinations

$$q = P_f - P_i$$

$$P = P_f + P_i$$

along with the scalar variable q^2. Now O_μ might be a scalar a vector, a tensor or a combination of these, thus the most general form for O_μ is

$$O_\mu = F_1(q^2)\gamma_\mu + F_2'(q^2)\sigma_{\mu\nu}q_\nu + F_3(q^2)P_\mu + F_4(q^2)q_\mu + F_5(q^2)\sigma_{\mu\nu}P_\nu$$

where $F_1(q^2)$ through $F_5(q^2)$ are scalar functions of q^2 only, because the Dirac equation for $w(P_i)$ and $\overline{w}(P_f)$ denies the other scalar forms such as $P_i\gamma^\mu$, P_f^2, $2(M^2 - P_f.P_i)$ etc. Also $\sigma_{\mu\nu}$ is a tensor while γ_μ is a vector. The pseudo quantities are not applicable simply by the fact that O_μ is not a pseudo vector or a pseudo scalar.

It can be shown that $F_5(q^2)\sigma_{\mu\nu}P_\nu$ yields terms like $F_1(q^2)\gamma_\mu$ and $F_4(q^2)q_\mu$, hence the $F_5(q^2)\sigma_{\mu\nu}P_\nu$ term can be neglected. Also $F_2'(q^2)\sigma_{\mu\nu}q_\nu$ and $F_3(q^2)P_\mu$ produce the same type contribution, therefore, the $F_2'(q^2)\sigma_{\mu\nu}q_\nu$ term is retained. By current conservation $\partial J_\mu/\partial x_\mu = 0$, the $F_4(q^2)q_\mu$ term can be eliminated. Thus the final general form of 0_μ is

$$0_\mu = F_1(q^2)\gamma_\mu + F_2'(q^2)\sigma_{\mu\nu}q_\nu \tag{13}$$

Now returning to equation (4) and replacing γ^ν by 0^ν as defined by equation (13) and repeating the previous mathematical difficulty, the well known Rosenbluth [1] formula is produced

$$\frac{d\sigma}{d\Omega} = \frac{e^4}{4E_i^2}\frac{\cos^2\theta/2}{\sin^4\theta/2}\left\{F_1^2 - \frac{\hbar^2q^2}{4M^2}\left[2(F_1+\kappa F_2)^2\tan^2\theta/2 + \kappa^2F_2^2\right]\right\} \times \frac{1}{1+\frac{2E_i}{Mc^2}\sin^2\theta/2} \tag{14}$$

If κ is set equal to zero and F_1 equal to unity, then equation (12) is reproduced.

3. PROTON FORM FACTOR

Electron-proton scattering results at intermediate values of momentum transfer are presented by Hand, Miller and Wilson [5] and Janssens [6] et al, among others.

Janssens' experimentally verified three pole approximation of the charge and magnetic form factors for the proton above q^2 of $4F^{-2}$ was shown to be in excellent agreement, after extrapolation, with previous experimental results below q^2 of $4F^{-2}$. This reveals that the form factors of the proton have the same dependence on q^2 within experimental accuracy in the region of q^2 less than $4F^{-2}$. Therefore, setting $F_1 = F_2$ in equation (14) and factoring yields

$$\frac{d\sigma}{d\Omega} = \frac{1}{E_i^2} \frac{e^4}{4} \frac{\cos^2 \theta/2}{\sin^4 \theta/2} \frac{F^2(q^2)}{1 + \frac{2E_i}{Mc^2} \sin^2 \theta/2}$$

$$\times \left\{ 1 + \frac{\hbar^2 q^2}{2M^2} \left[2(1 + \varkappa)^2 \tan^2 \theta/2 + \varkappa^2 \right] \right\} \qquad (15)$$

or

$$\frac{d\sigma}{d\Omega} = \left(\frac{d\sigma}{d\Omega}\right)_{\text{Rosenbluth}} \times F^2(q^2) \qquad (16)$$

In equation (15) the quantity

$$\frac{e^4 \cos^2 \theta/2}{4 \sin^2 \theta/2}$$

is Mott's cross section $(d\sigma/d\Omega)$ Mott for 1 MeV and is tabulated in Herman and Hofstadter's High Energy Electron Scattering Tables [7]. The term

$$\eta = 1 + \frac{2E_i}{Mc^2} \sin^2 \theta/2 \tag{17}$$

is the recoil factor and letting

$$K(q^2,\theta) = 1 + \frac{\hbar^2 q^2}{4Mc^2} 2(1 + \varkappa)^2 \tan^2 \theta/2 + \varkappa 2$$

then Rosenbluth's formula can be written

$$\left(\frac{d\sigma}{d\Omega}\right)_R = \frac{1}{E_i^2} \left(\frac{d\sigma}{d\Omega}\right)_{Mott} \times \frac{K(q^2,\theta)}{\eta(E_i,\theta)} \tag{18}$$

The above form is for ease of handling on a desk calculator but could be adapted quite easily for a computer program.

It was stated, in the theory, that due to Relativistic Quantum Mechanical definitions the form factor could be a function of q^2 only. Knowing this, different sets of incident energy, E_i, and scattering angle, θ, for which q remains the same, should give identical form factors, F, in the region below q^2 of $4F^{-2}$. Thus an excellent check of the internal consistency is possible.

4. RADIATIVE CORRECTIONS

Accompanying elastic scattering of electrons is a radiation of photons. This radiation can be real (the familiar bremstrahlung emitted by electrons emerging from a target of finite thickness) or virtual (multiple scattering within a target). Thus, the low energy side of an elastic peak will show a tail which decreases as the reciprocal of the energy of the emitted radiation.

The well known virtual emission and absorption of radiation during the act of scattering can be accounted for by a multiplicative correction of the experimental cross section. This was originally developed by Schwinger [8] assuming no recoil of the target nucleus. A more valid form considering recoil of the proton was developed by Tsai [9] and is

$$K_s = e^{\delta_s}$$

where

$$\delta_s = \frac{2\alpha}{\pi}\left\{\left[\ell n \frac{E_i}{\Delta E \eta^{3/2}} - \frac{13}{12}\right]\left[\ell n\left(\frac{2E_i Mc^2}{(mc^2)^2}\left(1 - \frac{1}{\eta}\right)\right)\right] + \frac{17}{36}\right\} \quad (19)$$

α is the fine structure constant ($\sim 1/137$), E_i the incident energy of the electrons, ΔE the difference between the most probable energy of the scattered electron and the energy of the scattered electron where data was terminated (note $\Delta E \geq 4\Gamma_s$ [10], where Γ_s is the full width at half maximum, FWHM, of the spectrum of the scattered electrons), η is the nuclear recoil factor, see equation 17, M is the rest mass of the target nucleus, c the velocity of light, and m is the rest mass of the incident electrons.

A correction for the emission of real radiation is also multiplicative and is attributed to Bethe and Ashkin [11]. It is given by

$$K_b = e^{\delta_b} .$$

If recoil effects are considered, δ_b is defined by equation (20) and is valid only if $\hbar q/c$ is less than the rest mass of the target nucleus.

$$\delta_b = \frac{t_o}{\ell n 2} \ell n \left(\frac{E_i}{\Delta E \eta} \right)^{3/2} \qquad (20)$$

t_o is the effective target thickness $t'_o/\cos \varphi$ in radiation lengths, φ the angle the target makes with the incoming beam, t'_o is the actual target thickness t, times the density of the target material ρ, divided by the radiation length X_o [10] of the target material (i.e., $t'_o = t\rho/X_o$).

5. EXPERIMENTAL SETUP

A beam of electrons from the NPGS Linac accelerator (LINAC) is incident on a target containing protons. Electrons scattered by the proton at a particular angle and with a particular final energy are detected.

The beam pulses have a width of 1 micro second; the repetition rate is 60 pulses per second. The beam emerges from the accelerator proper through a collimator of 3/16 inch diameter. The collimated beam then enters a double deflecting magnet system which bends the beam a total of 60 degrees with respect to the accelerator center line. A nuclear magnetic resonance device in the first deflection magnet determines the beam energy to better than 0.5%. Between the magnets in the deflection system, a set of adjustable slits is located which defines the relative energy spread in the beam. (See Midgarden's thesis December 1967, figure I [12]). The beam is monitored by a secondary emission monitor (SEM) consisting of 5 Aluminum foils of ½ mil thickness. The signal from this monitor indicates the beam current at the control console. The beam leaves the accelerator vacuum system through a 5 mil aluminum window and enters the evacuated target chamber to strike the target. The signal from a downstream SEM is integrated at the control console, yielding the number of electrons passing through the target. The beam is focussed at target center and has a diameter of approximately ¼ of an inch. The beam spot is viewed on a zinc sulfide screen via closed circuit television.

The target materials were polyethylene $(CH_2)_n$ and carbon. The net effect of the protons was obtained by subtracting the carbon

background. The polyethylene target is a disc rotated at either 2 or 4 revolutions per minute to prevent destruction by heat.

A ladder that can accommodate four targets selects a specific target by moving vertically and can rotate about the target center in a horizontal plane. (See figure II). Each motion is independently controlled from the monitoring area. In order to select a particular energy and angle of a scattered electron, a double focussing magnetic spectrometer is used. Its deflection angle is 120 degrees and its mean radius of curvature is 16 inches. The spectrometer is moved about the target center in a horizontal plane on a U. S. Navy twin 40 millimeter gun mount by local control. The energy setting is selected by a rotating coil fluxmeter, first developed by Bumiller [13], and its associated electronics. The readout of the fluxmeter is calibrated directly in MeV. A feedback system maintains the spectrometer's field setting constant to 1 part in 5000. This system is an improved version of that described by Kenaston [14].

Electrons scattered at a set angle enter the spectrometer as indicated in figure I. The spectrometer vacuum chamber and target chamber are coupled by a bellows and maintained at a vacuum of approximately 25 microns. The solid angle accepted by the spectrometer is determined by a tungsten entrance slit located 16 inches from the target. The slit is 1 1/2 inches high and 5/16 inch wide.

Electrons that enter the spectrometer are deflected and focussed into a counter house located under shielding on a platform fixed to the spectrometer. A slit at the spectrometer exit determines the energy spread accepted by the spectrometer. Figure I shows the spectrometer and counting system relative to the target.

To suppress background counts, a counter telescope is used. It consists of two counters in line with the electrons emerging through the energy slit. Both counters are NE102 plastic scintillation counters on Xp-1110 photo multipliers.

The counters work in coincidence into electronics described by Kenaston, Luke and Sones [14].

The original scalers used, in the first eight experiments, were unable to count more than one scattered electron per pulse, thus a correction to the observed counting rate was necessary in order to compensate for dead time losses in the scaler. By restricting the observed counting rate to less than five counts per second, this correction was never allowed to exceed 5.0%, which corresponds to a 1.0% correction for every count per second over one.

Scalers, which were ten to fifteen times faster than the original scalers, were used in the remaining experiments. A determination of their maximum counting rate is discussed under chapter 6.

A standardization target, carbon, was used since the integrating SEM provides only a relative measurement when not calibrated. At each setting of the spectrometer energy, after the elastic carbon peak was attained, the number of scattered electrons were recorded for both the carbon and polyethylene targets sequentially at each spectrometer setting. This was done to eliminate as much systematic error as possible.

6. CALCULATIONS OF EXPERIMENTAL CROSS SECTIONS

The experimental electron-proton cross section is calculated from the following equation:

$$\left\{\frac{d\sigma}{d\Omega}(E_i,\theta)\right\}_{Meas} = \frac{N_D}{N_i\, N_T\, t\, \Delta\Omega}\, K_s K_b A_o \qquad (21)$$

N_D is the number of scattered electrons detected, N_i the number of incident electrons, N_T the number of target nucleii per cm^3, t the effective target thickness, t'/cos φ, where t' is the actual thickness of the target and φ the angle the target makes with respect to the incoming beam, $\Delta\Omega$ is the solid angle defined by the slit on the entrance to the spectrometer, K_s and K_b the radiative correction factors, A_o is the normalization factor derived from the carbon data.

In the following paragraphs, an account is given on how each term of the cross section is obtained. A discussion of possible error sources for each of the quantities is presented.

N_D: A smooth curve is drawn through a plot of the coincidence counts versus spectrometer energy. (see figures III and IV). The separately measured carbon background is subtracted and the area under the curve, representing the proton counts, is determined in counts MeV. This number is then converted to the number detected, N_D, by dividing by the momentum acceptance, δ_p, of the spectrometer in MeV. The momentum acceptance is defined by the relation:

$$\frac{\delta p}{P_{sc}} = \frac{\delta s / r_o}{D} \qquad (22)$$

where P_{sc} is the most probable energy of the scattered electron in MeV, δs the exit slit width of the spectrometer (.078 in.), r_o the mean radius of curvature (16 inches), and D the dispersion of the spectrometer determined from an optics study by Oberdier [15] to be 3.9 ± 0.1.

The accuracy of N_D depends on the carbon subtraction, spectrometer calibration, counter efficiency, the number of counts, the momentum acceptance and beam positioning on the target.

The error introduced by carbon subtraction is mainly statistical and ranges from approximately 4% at a scattering angle of 45^o to 7% at 120^o.

Oberdier's study of electron trajectories in the spectrometer ("optics" study) measured the angle of inclination and the position of the focal plane, the energy calibration, and the dispersion. Thus the internal consistency of the spectrometer calibration is confirmed. Its absolute calibration was established relative to the incident energy of the electrons, using the relativistic kinematics of the scattering process and considering the energy loss in the target.

The proper setting of the coincidence timing for the front and back counters was determined by inserting a variable delay cable before each counter's input to this circuit. ("Cable curve" 14).

It was necessary to adjust the individual discriminator circuits along with the high voltage on each corresponding photomultiplier for optimum counting efficiency. The discriminator level and high voltage were selected by observing an elastic scattered electron spectrum of carbon. For each channel, the counting rate per unit charge passing through the target was recorded, first as a function of discriminator setting and then as a function of high voltage on the photomultiplier tube. Thus the plateau region of each counting circuit was determined. ("Plateau Curves" [16]). Then the center of each circuit's plateau was selected.

In the latter part of this work fast electronic scalers were used with a maximum count rate of 10 MHz. The maximum number of random counts per second that the scalers' would accept had to be determined. A Carbon peak at low scattering angle was taken with a counting rate of less than one per second. The beam current was then increased, retaining the position of the peak until a rate of 120 counts per second was obtained. At a counting rate of 15 per second, the total counts on the peak were still within statistics of the total counts on the peak at the rate of one per second. At 20 per second the total counts on the peak were approximately 5% lower than the statistical error at one per second. Therefore, no higher counting rate than 15 counts per second was allowed. However, the counting system had not been calibrated against a faster system and this lack of calibration can probably explain a major portion of the discrepancy between our carbon data obtained and those accepted in the literature.

The counting rate is assumed to follow Poisson statistics, therefore, the error in a single count is simply the square root of the number of counts for each point. These are plotted as error flags in figures III and IV.

The number of incident electrons N_i is measured by integration of the secondary electrons from the secondary emission monitor (SEM). Since all experiments performed were relative to carbon, no calibration of the SEM was required. However, a major portion of the discrepancy between our carbon data and those accepted in the literature can probably be explained by the lack of this calibration.

N_T: The densities of the carbon and polyethylene targets were determined to be $1.44 \pm .01$ gm/cm^3 and $0.922 \pm .005$ gm/cm^3 respectively. It is desirous to have a carbon partner for each polyethylene target that is to make the number of carbon atoms in carbon, n_c, to be equal to the number of carbon atoms in polyethylene, n_p. Using the formula

$$n = \frac{\rho N_o}{M}$$

Where ρ is the density and M the atomic or molecular weight of the target material; N_o is Avagadro's number. The rate of n_p to n_c is calculated using the above densities to be $1.82 \pm .02$.

The solid angle $\Delta\Omega$ is computed by dividing the area of the spectrometer entrance slits by the square of the distance from target center to this slit. The same slit opening (1 1/2" x 5/16") was used for all experiments yielding a solid angle of 1.381×10^{-3}

steradians. This assumes a point beam spot whereas the beam spot is finite (approximately ¼") in diameter. This finite beam size with the small distance of 16 inches can lead to appreciable counting losses since electrons from the outer fringes of the beam spot may not pass through the spectrometer.

A_o is the normalization factor obtained by taking a simultaneous elastic carbon peak and comparing our reduced carbon data with the cross section for carbon taken from the literature. To arrive at a value for a carbon cross section, the carbon form factor was computed from $F(q^2) = (1 - 0.3062q^2) \exp(-0.7310q^2)$ [17].

All measurements reported here are relative cross sections. Each proton measurement was preceded by a carbon measurement with identical experimental conditions. A total of nineteen matching elastic scattering curves of appearance comparable to that in figure III were taken. The elastic peak in figure IV was taken at a very low q^2 of $0.025F^{-2}$ and shows the lack of resolution. This lack of resolution is due to the spectrometer's resolution, finite beam size, initial energy spread of the beam and divergence of the beam in the target. Figure V is the proton peak obtained from figure IV by replotting the vertical separation between the polyethylene and carbon curves. The carbon backgrounds were taken separately using graphite targets.

7. EVALUATION OF DATA

Each experimental elastic peak taken, both the carbon and the proton, is evaluated. The literature value for the carbon cross section is determined using Ehrenberg's [17] form factor formula. The ratio of this value to the measured value for carbon is taken. This yields A_o for equation (21). Then the cross section of the elastic proton peak is evaluated using equation (21), this is $(d\sigma/d\Omega)_{Meas}$. The Rosenbluth cross section for the proton is determined using equation (18), this yields $(d\sigma/d\Omega)_R$. The proton form factor is obtained from the square root of the ratio of the measured cross section to the Rosenbluth cross section; that is

$$F_{proton} = \sqrt{\frac{(d\sigma/d\Omega)_{Meas}}{(d\sigma/d\Omega)_R}} \qquad (23)$$

The result of each experiment is tabulated in Table I under column 6. Column 8 is the charge form factor, F_{ch}, calculated from Janssens' three pole approximation [6].

TABLE I. THE FORM FACTOR AS A FUNCTION q^2

1	2	3	4	5	6	7	8
q^2	E_i	Ang	$K_s K_b$	A_o	F	<F>	F_{ch}
F^{-2}	MeV	deg					
.025	41.0	45	1.10	3.02	1.019±.007	1.019±.007	.997
.050	58.1	45	1.14	2.30	.882±.007	.839±.007	.994
.050	58.1	45	1.10	1.82	.792±.007		
.100	82.5	45	1.13	2.63	.845±.011	.858±.013	.988
.100	52.3	75	1.12	3.61	.932±.022		
.100	40.4	105	1.12	2.59	.833±.010		
.185	86.9	60	1.13	*7.32	.826±.015	.883±.024	.978
.185	71.6	75	1.13	*10.1	.930±.023		
.185	62.0	90	1.12	*9.47	.909±.026		
.185	51.0	120	1.10	*7.36	.899±.046		
.328	96.2	75	1.15	*6.00	.939±.040	.886±.034	.962
.328	83.3	90	1.14	*6.24	.898±.031		
.328	74.7	105	1.13	*9.30	.873±.035		
.328	68.7	120	1.12	*5.37	.827±.053		
.328	68.7	120	1.14	1.99	.876±.023		
.467	90.0	105	1.15	1.69	.955±.023	.911±.023	.946
.467	82.9	120	1.15	1.88	.863±.022		
.524	88.1	120	1.13	1.49	.917±.025	.917±.025	.940
.619	96.3	120	1.15	1.31	.994±.021	.994±.021	.930

* data taken using slower scalers

8. DISCUSSION OF DATA

Figure IV shows the individual data points from table I as compared to JANSSENS' three pole fit [7]. It is evident that the data do not fit to the curve. The trend exhibited in the position of the data points in the region of q^2 from 0 to $0.4F^{-2}$ shows the same shape as would be expected if the existence of a proton halo [3] would be assumed although the deviation from Janssens' fit is much too large. This large deviation could, however, be the result of a systematic error in the data used for the carbon normalization.

To exhibit the foregoing statements more clearly, the averaged data points are plotted in figure VII. In addition to Janssens' fit a curve representing the trend of the form factor under the assumption of a halo is also shown. This curve represents the function [3].

$$F = \frac{1 - \epsilon}{\left[1 + q^2 \frac{R_p^2}{12}\right]^2} + \frac{\epsilon}{\left[1 + q^2 \frac{R_H^2}{12}\right]^2}$$

with $\epsilon = 0.037$, $R_H = 6$ Fermis, $R_p = 0.85$ Fermis. Again it becomes clear that one cannot speak of a fit but only of a similar trend in the shape.

One remark of caution is in order here. If one accepts the speculation of the existence of a proton halo, the question arises, what influence does this halo have upon the form factor of the carbon nucleus. No theoretical studies of this problem have been carried out so far, but it is possible that there might be an appreciable influence on the carbon normalization.

9. CONCLUSIONS

It is quite clear from the scattering of the individual data points that experiments of considerably higher accuracy must be performed. It will especially be necessary to improve experimental techniques to a degree that allows proton data to be taken absolutely instead of relative to carbon. Improvements in this direction have already been made during the course of the present experiment as evidenced by a decreasing carbon normalization factor A_o.

Analysis of the data scattering, however, does not show any systematic way by which the shape of the data curve could be adjusted closer to the accepted fit by Janssens.

The only conclusion we can draw so far is that the data do not exclude the possibility of the existence of a proton halo. The same conclusion, incidentally, must be made considering all other proton form factor data in a range of momentum transfers comparable and slightly higher than the present one [3].

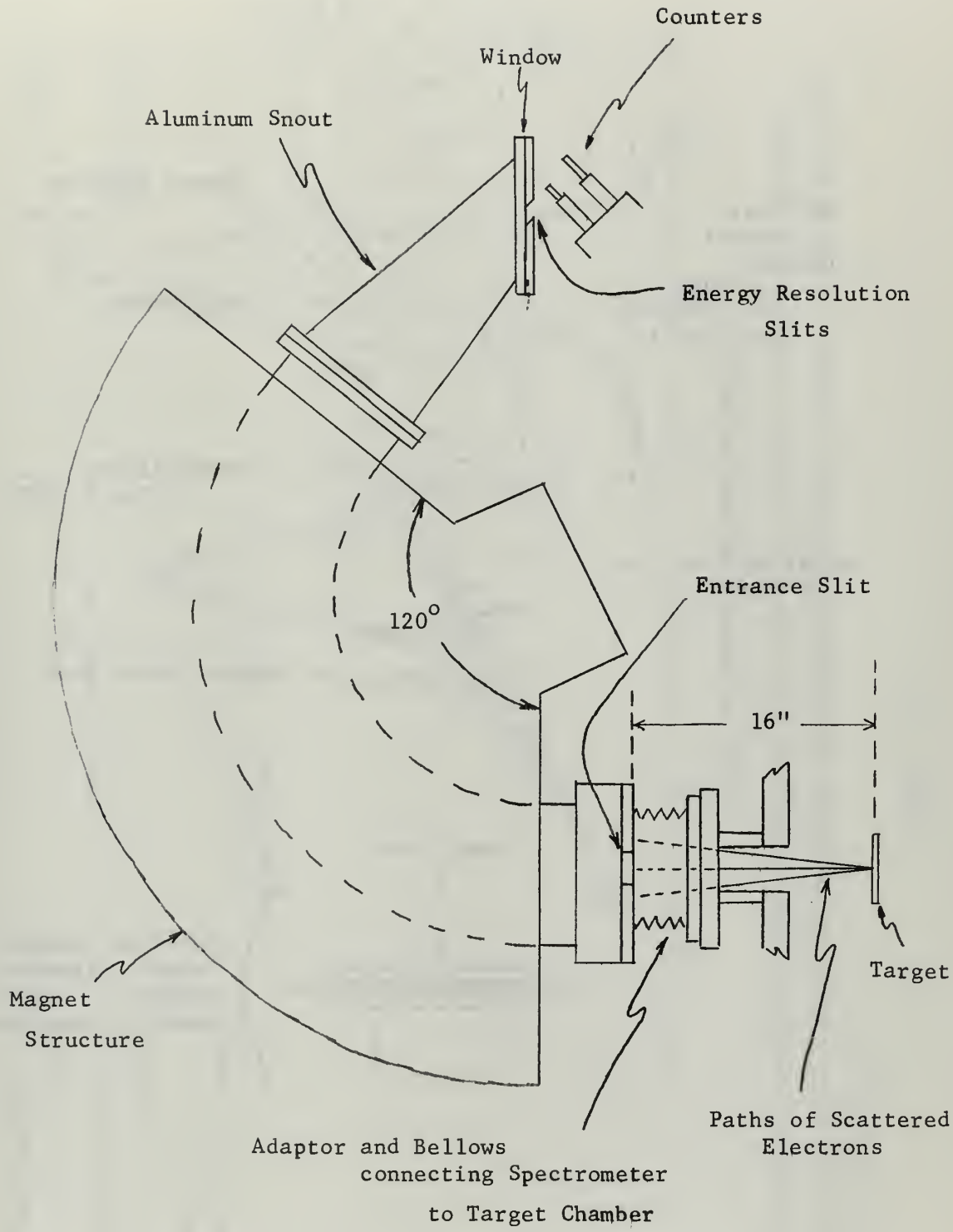
Counters
Window
Aluminum Snout
Energy Resolution
Slits
120°
Entrance Slit
16"
Target
Magnet
Structure
Adaptor and Bellows
connecting Spectrometer
to Target Chamber
Paths of Scattered
Electrons

Figure - I

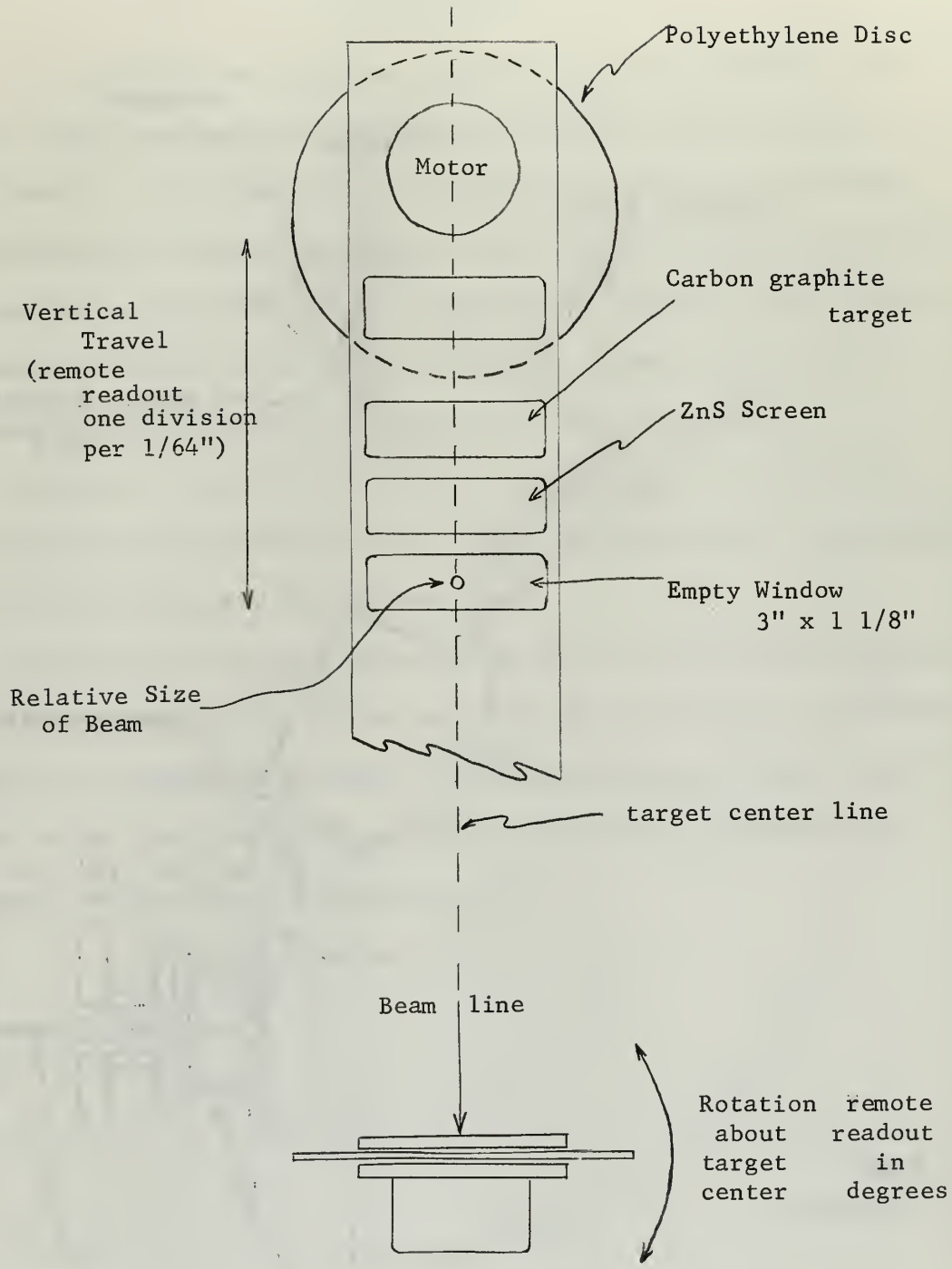
Polyethylene Disc
Motor
Carbon graphite target
Vertical Travel (remote readout one division per 1/64")
ZnS Screen
Empty Window 3" x 1 1/8"
Relative Size of Beam
target center line
Beam line
Rotation about target center
remote readout in degrees

Figure - II

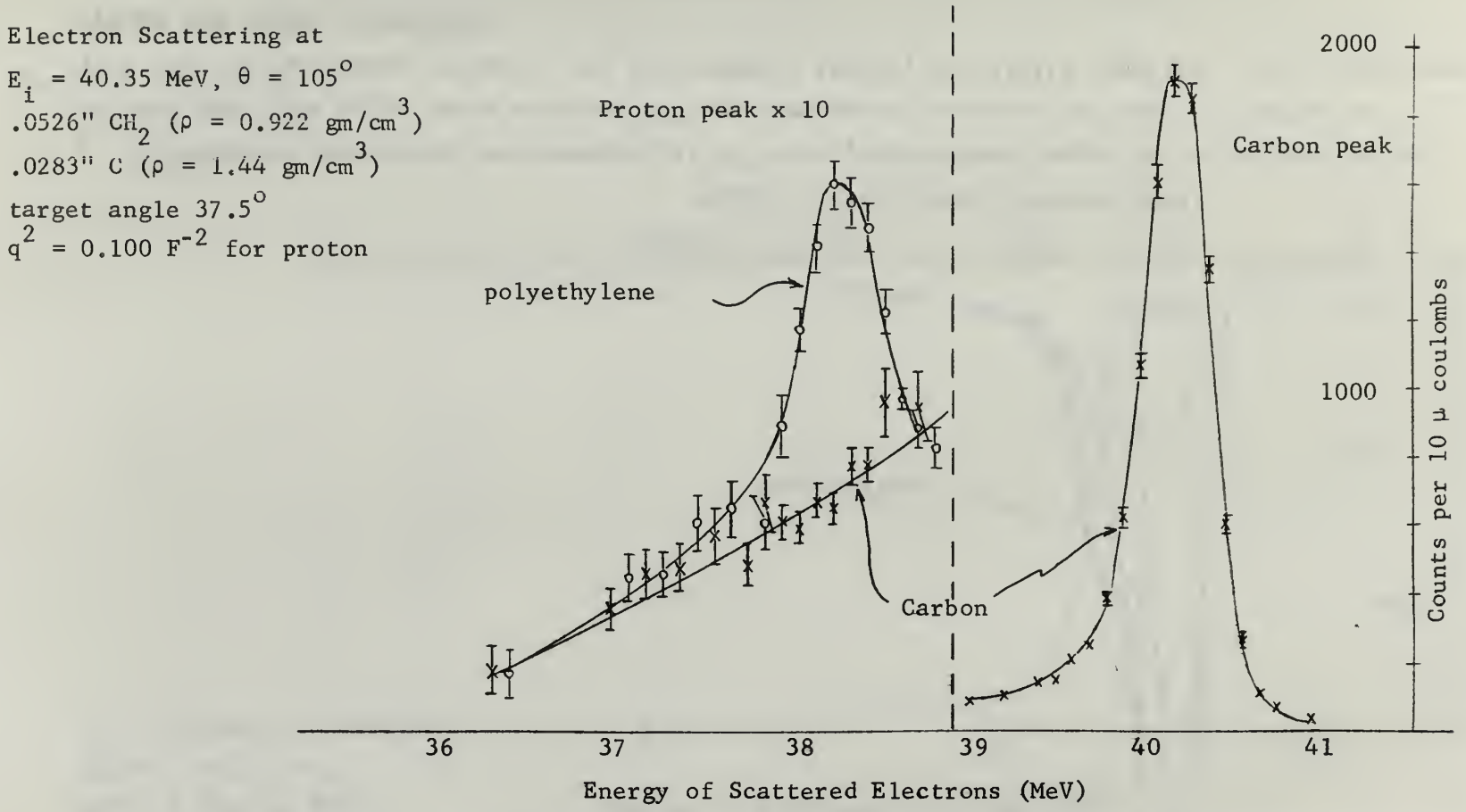

An electron scattering peak observed at 105° from a polyethylene target at an incident energy of 40.35 MeV. This curve indicates the quality of the peaks obtained at other than very low q^2 for the proton.

Figure - III

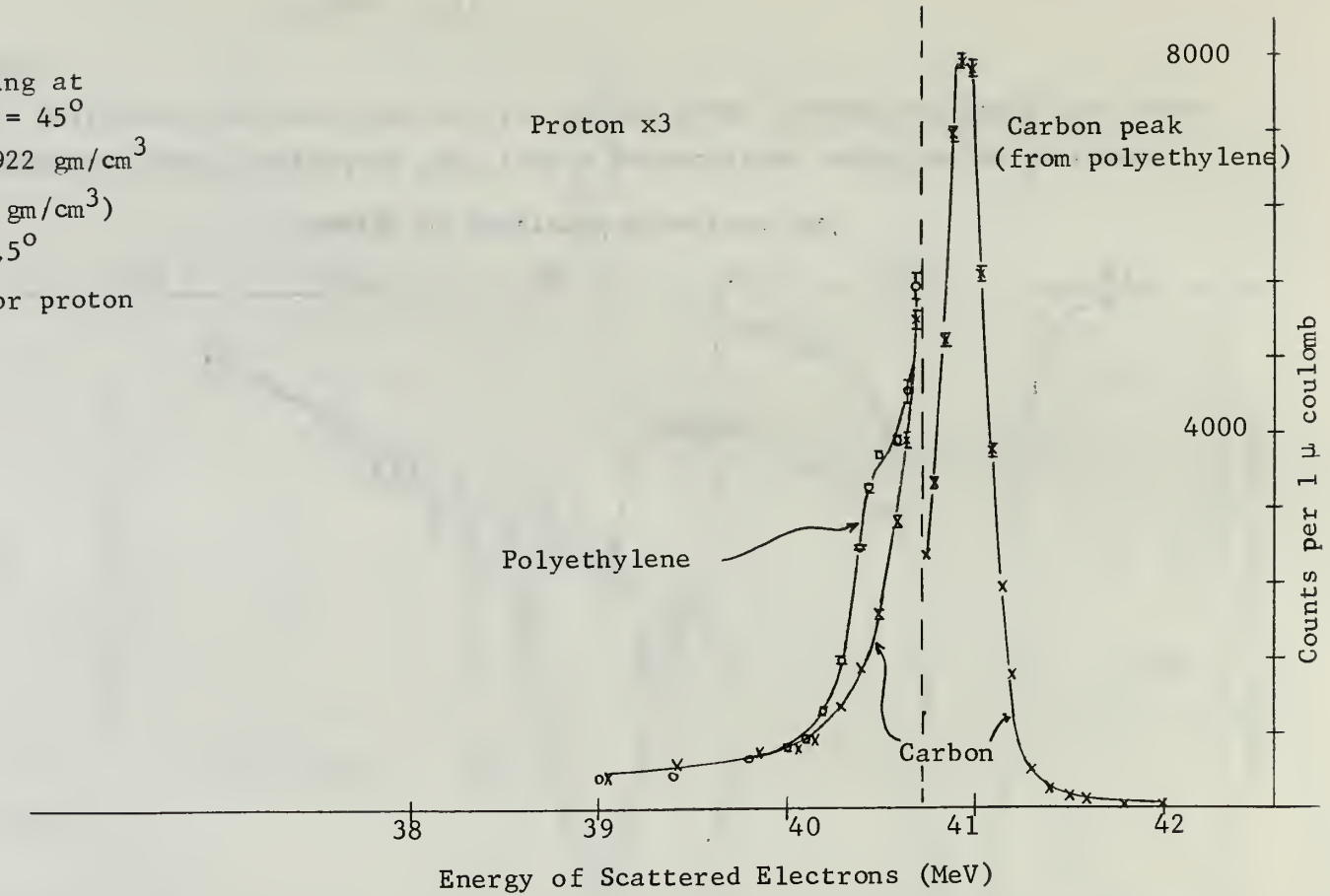

An electron scattering peak observed at 45° from polyethylene target at an incident energy of 41.0 MeV. The curve taken with the 16" spectrometer illustrates the lack of resolution. This lack of resolution is due to the spectrometer itself, the finite beam size, the initial beam spread and target spreading.

Figure -IV

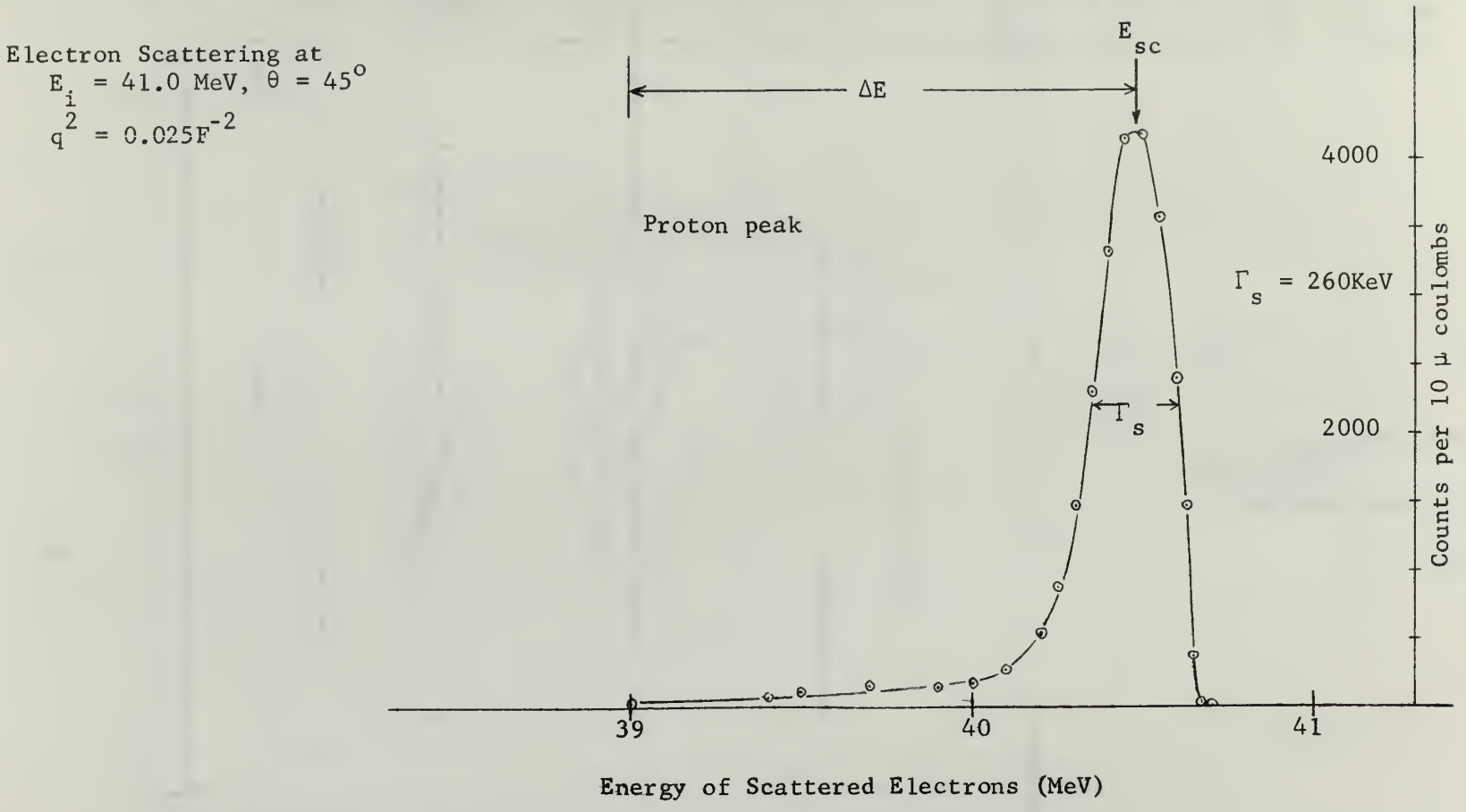

Proton peak unfolded from Figure - by replotting vertical separation

Figure - V

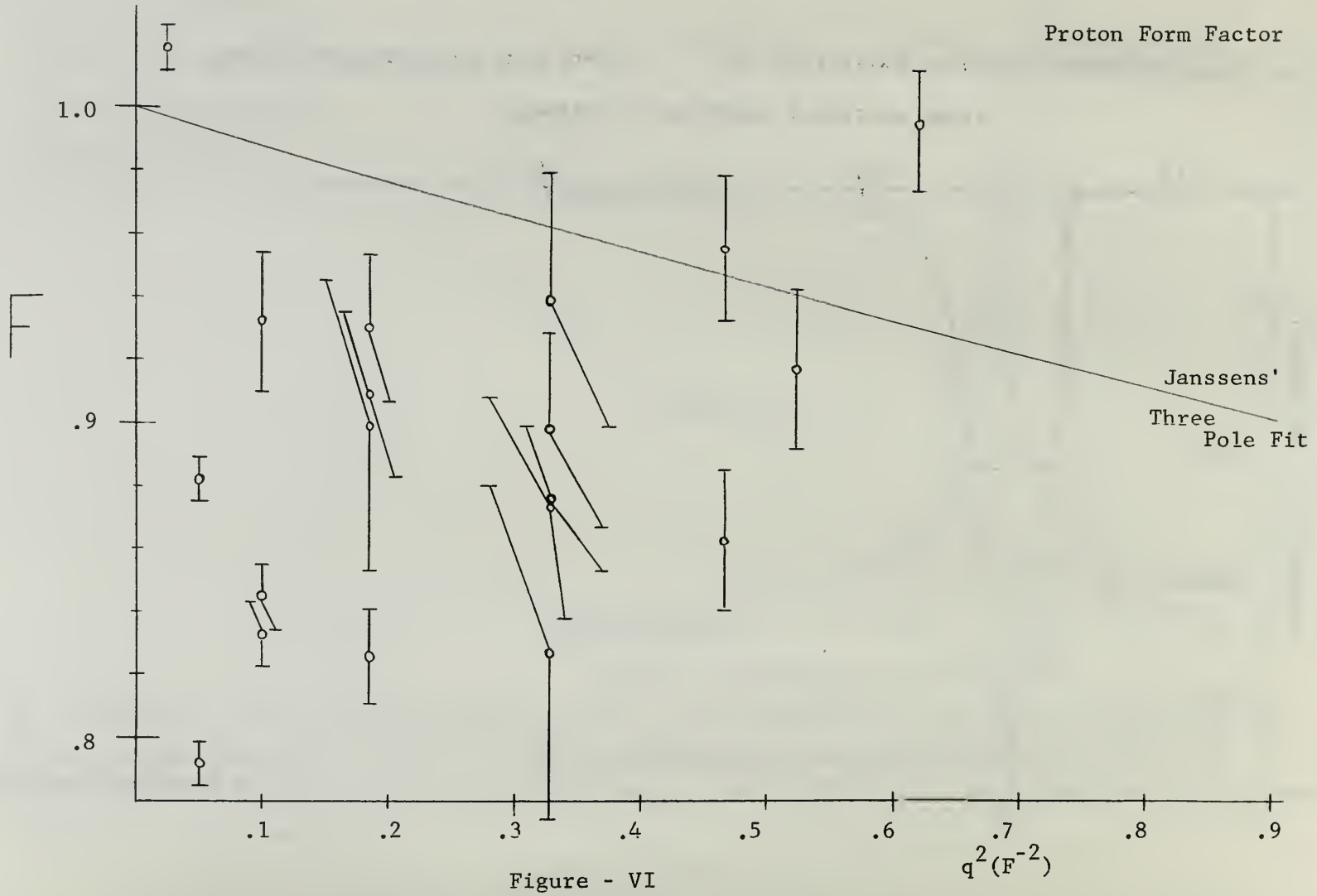
Proton Form Factor
1.0
.9
.8
F
Janssens'
Three
Pole Fit
.1
.2
.3
.4
.5
.6
.7
.8
.9
$q^2(F^{-2})$

Figure - VI

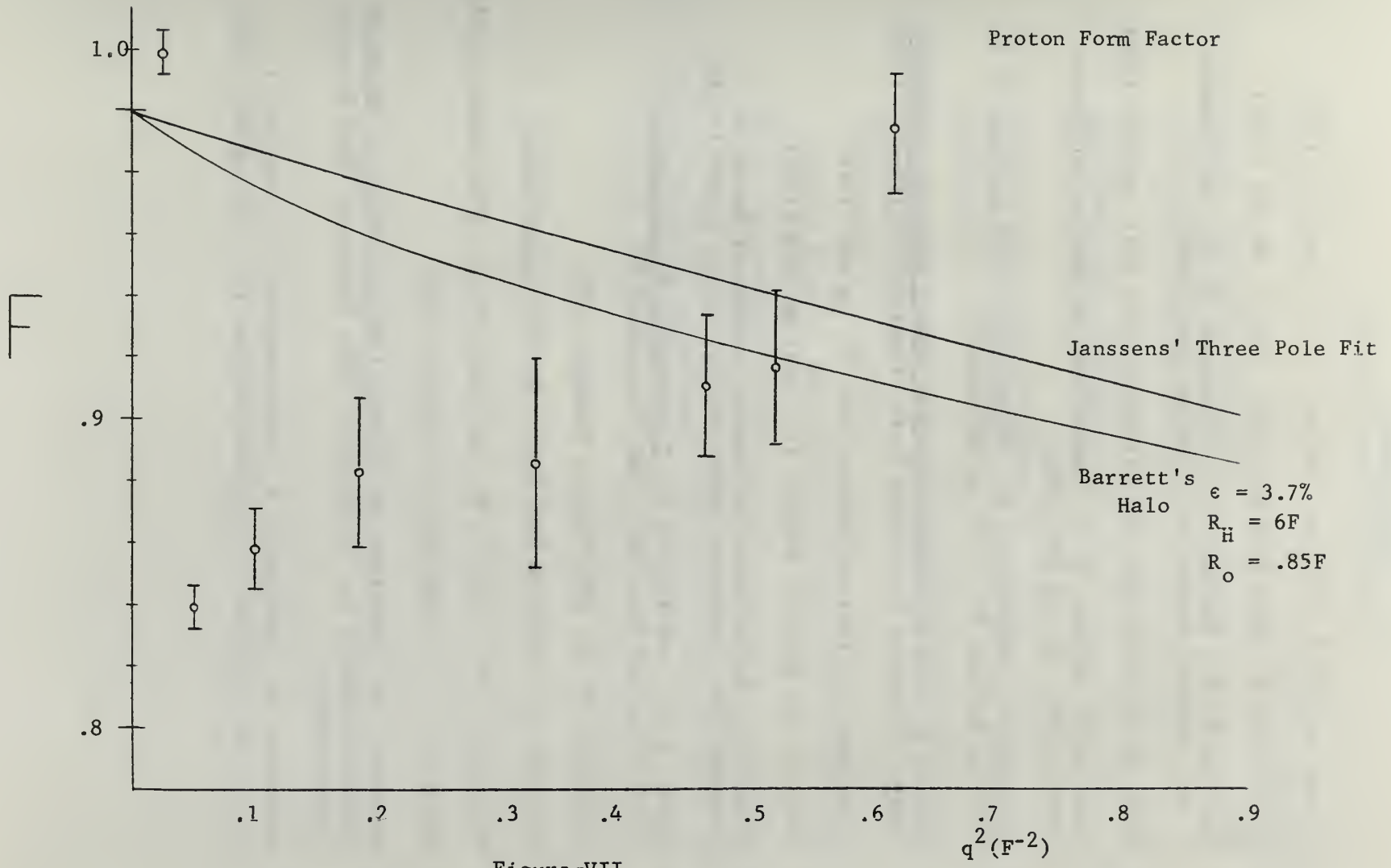
Proton Form Factor
1.0
.9
.8
F
Janssens' Three Pole Fit
Barrett's
Halo
ε = 3.7%
R_H = 6F
R_o = .85F
.1
.2
.3
.4
.5
.6
.7
.8
.9
$q^2(F^{-2})$

Figure-VII

BIBLIOGRAPHY

1. Rosenbluth, M. N., Physical Review, Vol. 79, pg 615 (1950).

2. Hofstadter, R., Ann. Rev. Nuc. Sci., Vol. 7, pg 231 (1957).

3. Barrett, R. C., Brodsky, S. J., Erickson, G. W., and Goldhaber, M. H., Physical Review, Vol. 166, pg 1589 (1968).

4. Mott, N. F., Proc. Roy. Soc. (London), Vol. A117, pg 610 (1928).

5. Hand, L. N., Miller, D. G., and Wilson, R., Reviews of Modern Physics, Vol. 35, pg 335 (1963).

6. Janssens, T., Hofstadter, R., Hughes, E. B., and Yearian, M. R., Physical Review, Vol. 142, pg 922 (1966).

7. Herman, R., and Hofstadter, R., High Energy Electron Scattering Tables, (Stanford University Press, Stanford, California) (1960).

8. Schwinger, J., Physical Review, Vol. 75, pg 898 (1949).

9. Tsai, Y. S., Physical Review, Vol. 122, pg 1898 (1961).

10. Breuer, H., Saskatchewan Accelerator Laboratory Report No. 4., December 1964, Saskatoon, Saskatchewan, Canada (unpublished).

11. Bethe, H. A., and Ashkin, J., Experimental Nuclear Physics (John Wiley and Sons, Inc., New York, 1953) Vol. 1.

12. Midgarden, P. N., NPGS Thesis, December 1967.

13. Bumiller, F., Stanford HEPL Report No. 257 (unpublished).

14. Kenaston, G. W., Luke, C. T., and Sones, W. C., NPGS Thesis (1965).

15. Oberdier, L. D., NPGS Thesis, September 1967.

16. Stroetzel, M., Institute For Technical Nuclear Physics, Darmstadt Laboratory Report No. 19, December 1965, Darmstadt, West Germany (unpublished).

17. Ehrenberg, H., Hofstadter, R., Meyer-Berkhout, U., Ravenhall, D. G., and Sobottka, S., Physical Review, Vol. 113, pg 666 (1959).

INITIAL DISTRIBUTION LIST

		No. Copies
1.	Defense Documentation Center Cameron Station Alexandria, Virginia 22314	20
2.	Library Naval Postgraduate School Monterey, California 93940	2
3.	Defense Atomic Support Agency Department of Defense Washington, D. C. 20301	1
4.	Commander, Naval Air Systems Command Department of Navy Washington, D. C. 20360	1
5.	Professor Franz A. Bumiller Department of Physics Naval Postgraduate School Monterey, California 93940	12
6.	Lt. Robert H. Gordon USN 1619 Rockwell Road Abington, Pennsylvania 19001	1

DOCUMENT CONTROL DATA - R & D

Security classification of title, body of abstract and indexing annotation must be entered when the overall report is classified)

1. ORIGINATING ACTIVITY (Corporate author)
Naval Postgraduate School
Monterey, California 93940

2a. REPORT SECURITY CLASSIFICATION
Unclassified

2b. GROUP

3. REPORT TITLE
Measurement of the Proton Form Factor at Low Momentum Transfer

4. DESCRIPTIVE NOTES (Type of report and, inclusive dates)
Master's thesis, June 1968

5. AUTHOR(S) (First name, middle initial, last name)
Robert H. Gordon

6. REPORT DATE	7a. TOTAL NO. OF PAGES	7b. NO. OF REFS
June 1968	43	17

8a. CONTRACT OR GRANT NO.	9a. ORIGINATOR'S REPORT NUMBER(S)
b. PROJECT NO.	
c.	9b. OTHER REPORT NO(S) (Any other numbers that may be assigned this report)
d.	

10. DISTRIBUTION STATEMENT
[redacted]

11. SUPPLEMENTARY NOTES	12. SPONSORING MILITARY ACTIVITY
	Naval Postgraduate School Monterey, California 93940

13. ABSTRACT

Electron scattering experiments on the proton were carried out in a range of momentum transfers squared of 0.025 (Fermi^{-2}) to 0.65 (Fermi^{-2}).

Polyethylene was used as target material and the proton data were normalized against carbon electron scattering data taken at higher momentum transfer.

The relative proton data obtained in this manner do not fit the generally accepted form factor curve.

Possible reasons for the deviations in view of recent suggestions about the existence of a proton halo are offered. However, it is not possible at the present stage of accuracy to make any definite statement except that the data are not inconsistent with the existence of a proton halo.

14. KEY WORDS	LINK A		LINK B		LINK C	
	ROLE	WT	ROLE	WT	ROLE	WT
Proton						
Form Factor						
Momentum Transfer						

thesG5748
DUDLEY KNOX LIBRARY
3 2768 00414792 6
DUDLEY KNOX LIBRARY